JACS
JOURNAL OF THE AMERICAN CHEMICAL SOCIETY
Article
Cite This: J. Am. Chem. Soc. 2018, 140, 18208−18216
pubs.acs.org/JACS

Bioinspired Metal−Organic Framework Catalysts for Selective Methane Oxidation to Methanol

Jayeon Baek,[†,‡,§,∥,○] Bunyarat Rungtaweevoranit,[†,‡,§,⊥,○] Xiaokun Pei,[†,‡,§,⊥] Myeongkee Park,[▽] Sirine C. Fakra,[#] Yi-Sheng Liu,[#] Roc Matheu,[†,‡,§,⊥] Sultan A. Alshmimri,[■] Saeed Alshehri,[■] Christopher A. Trickett,[†,‡,§,⊥] Gabor A. Somorjai,*[,†,∥,⊥] and Omar M. Yaghi*[,†,‡,§,⊥]

[†]Department of Chemistry, [‡]Kavli Energy NanoSciences Institute at Berkeley, and [§]Berkeley Global Science Institute, University of California—Berkeley, Berkeley, California 94720, United States

[∥]Chemical Sciences Division, [⊥]Materials Sciences Division, and [#]Advanced Light Source, Lawrence Berkeley National Laboratory, Berkeley, California 94720, United States

[▽]Department of Chemistry, College of Natural Science, Dong-A University, Busan 49315, Republic of Korea

[■]King Abdulaziz City for Science and Technology, Riyadh 12354, Saudi Arabia

Supporting Information

ABSTRACT: Particulate methane monooxygenase (pMMO) is an enzyme that oxidizes methane to methanol with high activity and selectivity. Limited success has been achieved in incorporating biologically relevant ligands for the formation of such active site in a synthetic system. Here, we report the design and synthesis of metal−organic framework (MOF) catalysts inspired by pMMO for selective methane oxidation to methanol. By judicious selection of a framework with appropriate topology and chemical functionality, MOF-808 was used to postsynthetically install ligands bearing imidazole units for subsequent metalation with Cu(I) in the presence of dioxygen. The catalysts show high selectivity for methane oxidation to methanol under isothermal conditions at 150 °C. Combined spectroscopies and density functional theory calculations suggest bis(μ-oxo) dicopper species as probable active site of the catalysts.

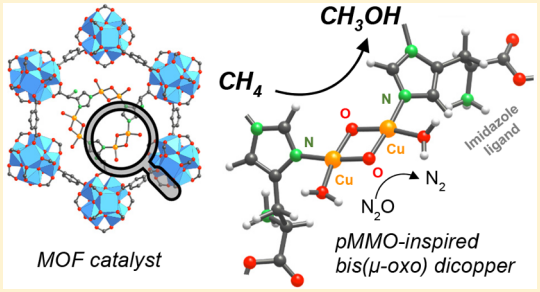

INTRODUCTION

Selective methane oxidation to methanol represents an important challenge in catalysis due to the difficulty in activating the strong C−H bond of methane (bond dissociation energy = 104 kcal mol^{-1}), giving rise to selectivity and activity problems.[1−8] Finding a solution to this impediment is a key toward the direct synthesis of methanol from methane.[9−11] In nature, particulate methane monooxygenase (pMMO) is an effective catalyst for the oxidation of methane to methanol.[12] Extensive studies on the pMMO suggest that the active sites are composed of copper complexes coordinated to histidines, although the nuclearity and the definitiveness of their structures remain a subject of debate.[12−15]

Inspired by pMMO, molecular complexes have utilized the tunability of ligand design in pursuit of duplicating the structure and reactivity in a synthetic system. A library of compounds with various copper−oxygen complexes have been reported, including but not limited to Cu_2O_2 [*trans*-1,2-peroxo, μ-η^2:η^2-peroxo and bis(μ-oxo)dicopper cores] and Cu_2O [mono(μ-oxo) dicopper core] along with their spectroscopic fingerprints.[16−18] Despite such a vast library of compounds, the reactivity of this class of catalysts is generally limited to substrates with weak C−H bonds due to the restricted thermal stability.[19] At elevated temperatures, these compounds are susceptible to decomposition via ligand oxidation and thus the loss of catalytically active copper−oxygen cores.[20] Although there exist synthetic catalysts capable of partial methane oxidation such as Cu-exchanged zeolites, the diversity of the active sites is limited to mono(μ-oxo)dicopper and tris(μ-oxo)tricopper cores.[3,5,21] In the gas phase, these catalysts typically operate in stepwise treatment for partial methane oxidation: (1) catalyst oxidation, (2) methane activation, and (3) methanol extraction, proceeding at different reaction temperatures, thus presenting a challenge for a streamlined catalytic process. Comparatively, oxidation of methane in the liquid phase where H_2O_2 is used as an oxidant, despite exhibiting high conversion, suffers from overoxidation of methanol yielding a mixture of methyl peroxide, formic acid, and carbon dioxide.[1,2,22]

The active sites of metalloenzymes are typically enclosed in a pocket for environmental control, hydrogen bonding, ion transport, or controlling the reaction to prevent self-destruction.[23−27] We envisaged that metal−organic frameworks (MOFs)[28] can serve as a scaffold akin to the polypeptide chains in enzymes whose arrangement of secondary and

Received: October 25, 2018
Published: December 10, 2018

DOI: 10.1021/jacs.8b11525
J. Am. Chem. Soc. 2018, 140, 18208−18216

tertiary structures can be achieved by judicious choice of structure and topology of MOFs.[29−32] The metal binding ligands bearing an imidazole unit in the copper active site of pMMO can be mirrored in a synthetic system by postsynthetic modification of MOFs.[33−35] Once these metal-binding ligands are in place, metalation with the desired configuration can be accomplished.[36,37]

Here, we demonstrate how a MOF can be used as a backbone for the creation of an enzyme-like active site by installing biologically relevant imidazole moieties, then subsequently metalating these ligands to incorporate reactive copper−oxygen complexes within the framework. From structural analysis of various MOFs, MOF-808, $Zr_6O_4(OH)_4(BTC)_2$ $(HCOO)_5(H_2O)_1(OH)_1$,[38] was selected as it possesses the chemical and geometric parameters for postsynthetic modifications to create the active sites inspired by pMMO. The resulting catalysts are capable of highly selective oxidation of methane to methanol under isothermal conditions. We identified the structure of the active sites using solid-state UV−vis, resonance Raman, and X-ray absorption spectroscopies complemented by density functional theory (DFT) calculations.

EXPERIMENTAL METHODS

Further details are available in the Supporting Information.

Synthesis of MOF-808. MOF-808 was synthesized following the reported procedure.[39] In a 100 mL media bottle were dissolved 1,3,5-benzenetricarboxylic acid (210 mg) and $ZrOCl_2{\cdot}8H_2O$ (970 mg) in a solution containing DMF (30 mL) and formic acid (30 mL). The bottle was sealed and heated in a 100 °C isothermal oven for a day. White powder was collected by centrifugation (8000 rpm, 3 min), washed with DMF three times (60 mL × 3) over a 24 h period, and then washed with acetone three times (60 mL × 3) over a 24 h period. Finally, MOF-808 was dried under dynamic vacuum overnight at room temperature. Anal. Calcd for $Zr_6O_4(OH)_4(C_9H_3O_6)_2(HCOO)_5(H_2O)(OH)(C_3H_7NO)_{0.5}$: C, 21.17; H, 1.56; N, 0.50. Found: C, 21.18; H, 1.37; N, 0.44.

Synthesis of MOF-808-Bzz. A solution of 5-benzimidazolecarboxylic acid was prepared by dissolving 5-benzimidazolecarboxylic acid (3 g) in DMSO (100 mL) in a 250 mL bottle in a 100 °C isothermal oven. MOF-808 (0.5 g) was suspended by sonication in the solution of 5-benzimidazolecarboxylic acid, and the suspension was heated in a 100 °C isothermal oven overnight. The reaction was allowed to cool to room temperature. Brown powder was collected by centrifugation (8,000 rpm, 3 min), washed with DMSO five times (80 mL × 5) over 3 days, and then with acetone five times (80 mL × 5) over 3 days. Finally, MOF-808-Bzz was dried under dynamic vacuum overnight at room temperature. Anal. Calcd for $Zr_6O_4(OH)_4(C_9H_3O_6)_2(C_8H_5N_2O_2)_{3.4}(HCOO)_{1.6}(OH)_1(H_2O)_1$: C, 32.15; H, 1.82; N, 5.45. Found: C, 31.07; H, 2.61; N, 5.30.

Synthesis of MOF-808-Bzz-Cu. A solution of CuI (99.999% metals basis, 81.6 mg) in ACN (12.8 mL) was added to a suspension of MOF-808-Bzz (75 mg) in ACN (1.9 mL) in a 20 mL vial while stirring (500 rpm) under ambient conditions. The vial was sealed, and the mixture was stirred for 3 days at room temperature. Brown powder was collected by centrifugation (8000 rpm, 3 min) and washed with ACN five times (15 mL × 5) over 3 days. Finally, MOF-808-Bzz-Cu was dried under dynamic vacuum overnight at room temperature. ICP analysis: Cu/Zr molar ratio = 1.2.

Catalysis. The catalytic testing was performed using a custom-designed continuous flow tubular reactor (Parr Instrument Co.). Mass flow controllers were calibrated using an ADM 1000 flow meter (Agilent Technologies) and ultrahigh purity He; CH_4 (Research 5.0 grade, Airgas) and 3% N_2O/He (Primary Standard grade, Praxair) were flowed into a 30 cm long quarter inch 316-stainless steel reactor. The catalyst (100 mg) was sieved to 100−250 μm and placed in the middle of the reactor tube, delimited by a layer of purified glass wool and a layer of quartz sand (50−70 mesh) at each end. Pretreatment of the catalyst was conducted under He (30 sccm) at 150 °C (3 °C/min) for 1 h. The catalyst was then oxidized using 3% N_2O/He flow (30 sccm) at 150 °C for 2 h. After being purged with He (30 sccm) for 30 min, CH_4 (30 sccm) was flowed into the catalyst for 1 h. After purging with He (50 sccm) for 1 h, 3% steam/He (30 sccm) was flowed into the catalyst. All lines were heated at 120 °C to prevent condensation. The outlet of the reactor was analyzed by gas chromatography (model GC-2014, Shimadzu Co.). The measurement started 3 min after opening the valve to 3% steam/He. The reactants and products were separated using a HayeSep R 80/100 stainless steel packed column (12 ft, 1/8 in OD, 2 mm ID). The water and CO_2 were monitored using a thermal conductivity detector, and methanol was monitored using a flame ionization detector.

X-ray Absorption Spectroscopy (XAS). N K-edge X-ray absorption spectra were collected at beamline 8.0.1, an undulator beamline with energy range of 80−1200 eV of the Advanced Light Source (ALS) at Lawrence Berkeley National Laboratory (LBNL). Its spherical gratings monochromator delivers 1012 photons/s with linear polarization with a resolving power up to 6000. The experimental energy resolution is better than 0.15 eV. Experiments were performed at room temperature. All of the spectra were collected in both total-electron-yield (TEY) and total-fluorescence-yield (TFY) modes simultaneously, corresponding to a probe depth of about 10 and 100 nm, respectively. We present spectra of TFY modes in this work as bulk measurement is preferred for our samples. The MOF-808-L-Cu samples were cooled with a He purge after each gas treatment in a 316-stainless steel reactor. The reactor containing the sample was sealed with a Swagelok valve and moved to an argon-filled glovebox (H_2O and O_2 levels <1 ppm). The sample was unloaded and pressed onto an indium foil using a hand press. Thereafter, these samples were transferred into an ultrahigh vacuum XAS end station (10^{-9} Torr) through our dedicated sample transfer kit to avoid air exposure. Energies were aligned by periodically collecting Ti L-edge spectra of a TiO_2 (anatase) reference for N K-edge. The XAS spectra were recorded over a wide energy range covering energies well below and above sample absorptions. The normalization was performed following the established procedure: (1) I_0-Normalization, the sample signal is divided by the incident intensity measured from the sample drain current from a freshly coated gold mesh inserted into the beam path before the X-rays can impinge on the sample. (2) A linear, sloping background is removed by fitting a line to the flat low energy region of the XAS spectrum, that is, at energies below any absorption peaks. (3) The spectrum is normalized by setting the flat low energy region to zero and the post edge to unity (unit edge jump).

Cu K-edge X-ray absorption spectroscopy data were collected at the Advanced Light Source (ALS) bending-magnet beamline 10.3.2 (2.1−17 keV) with the storage ring operating at 500 mA and 1.9 GeV, using a Si(111) monochromator and adjustable premonochromator slits.[40] All data were collected at room temperature (24 °C) in fluorescence mode at the Cu K-edge (8980.48 eV). The incoming X-ray intensity (I_0) was measured in an ion chamber and the fluorescence emission with a seven-element LN_2 cooled Ge solid-state detector (Canberra) using XIA electronics. Cu foil was used to calibrate the monochromator, with first derivative maximum set at 8980.48 eV,[41] and an internal I_0 glitch (present in all spectra) was used to calibrate the data. The MOF-808-L-Cu samples were cooled with a He purge after each gas treatment in a 316-stainless steel reactor. The reactor containing the sample was sealed with a Swagelok valve and moved to an argon-filled glovebox (H_2O and O_2 levels <1 ppm). The sample was unloaded and sealed with Kapton tape for ex situ measurements. Cu K-edge XANES spectra were recorded in fluorescence mode by continuously scanning the Si (111) monochromator (Quick XAS mode) from 8880 to 9020 eV, with 0.3 eV steps in the XANES region. All data were processed using the LabVIEW custom BL 10.3.2 software to perform dead time correction, energy calibration, and glitch removal with detail procedure described elsewhere.[42] XANES spectra were processed with Athena software61 to find the first derivative peak (E_0), pre-edge background subtraction and postedge normalization, and then align

DOI: 10.1021/jacs.8b11525
J. Am. Chem. Soc. 2018, 140, 18208−18216

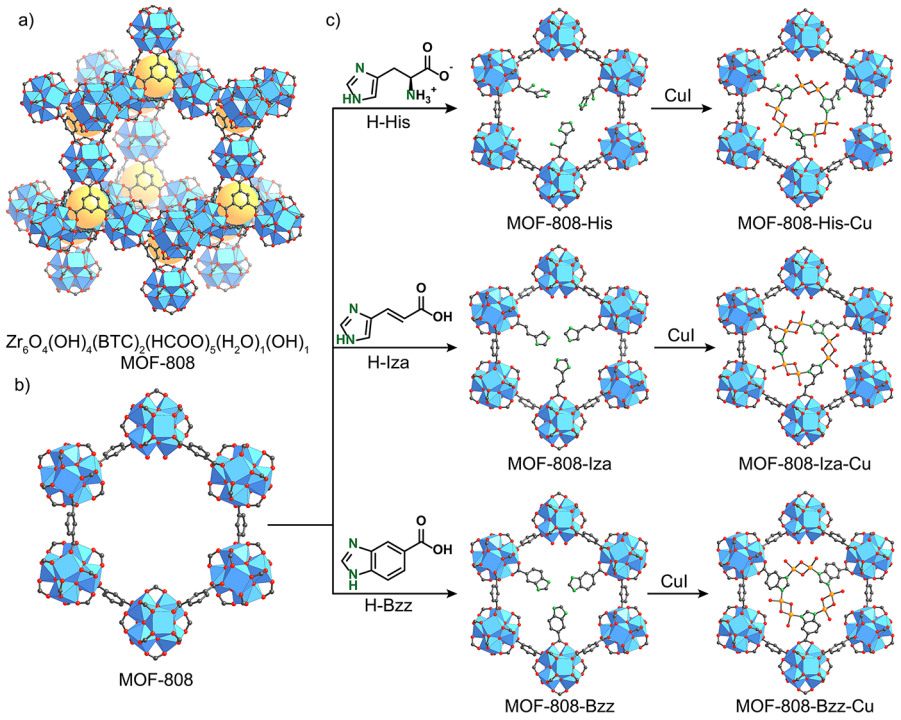

Figure 1. Design and synthesis of the catalysts bearing copper−oxygen complexes in MOF-808 for methane oxidation to methanol. (a) Structure of MOF-808. (b) Pseudohexagonal pore opening of MOF-808. (c) Synthesis of the catalysts comprising the replacement of formate with imidazole-containing ligands and metalation with Cu(I). Atom labeling scheme: C, black; O, red; N, green; Cu, orange; Zr, blue polyhedra. H atoms are omitted for clarity. Orange spheres represent the space in the tetrahedral cages.

and merge the spectra. EXAFS spectra were recorded up to 565 eV above the edge (8880−9545 eV, i.e., up to $k \approx 12$ Å^{-1}), and 11 scans were averaged. EXAFS spectra of samples were reduced with k^1-, k^2-, and k^3-weighting, out to $k = 10$ Å^{-1}, and analyzed via shell-by-shell fitting using the FEFF6l code and the Artemis software where it yields minima in variances.[43,44]

Resonance Raman Spectroscopy. In an argon-filled glovebox, a solution of CuI (6.25 mg) dissolved in anhydrous ACN (0.98 mL) was added to a suspension of MOF-808-Bzz (5.77 mg) in anhydrous ACN (0.14 mL) in a 1.5 mL GC autosampler vial equipped with a PTFE/rubber septum. The vial was sealed and removed from the glovebox. Either $^{16}O_2$ (Praxair, 99.999%) or $^{18}O_2$ (Aldrich, 99 atom %) was bubbled through the solution using a needle pierced through the septum at a rate of ca. 30 mL min^{-1} for 10 min. The suspension was allowed to react at room temperature for 3 days. The solid was collected by centrifugation, dried overnight, transferred to an argon-filled glovebox, and washed with anhydrous ACN five times (2 mL × 5) over 3 days. The sample was dried under dynamic vacuum overnight at room temperature, and the dried solid was transferred back to the glovebox. The sample was loaded into a thin-wall quartz capillary tube and sealed with epoxy glue for the measurements. All spectra were collected using the 407 nm light with the power density of 3.1 W/cm^2. The Raman scattering was collected using a Spex 1401 double grating spectrograph and liquid nitrogen cooled Roper Scientific LN/CCD 1100 controlled by a ST133 controller. The measured Raman shifts were calibrated by using Raman peaks of cyclohexane.

DFT Calculations. The clusters were geometrically optimized at the density functional theory (DFT) in the gas phase using spin-unrestricted B3LYP functional[45,46] as implemented in *Gaussian 16* (revision A03) without symmetry constraints.[47] The 6-31G basis sets were employed for C and H atoms, while 6-311G(d) basis sets were used for Cu, N, and O atoms. Numerical integrations were performed on an ultrafine grid. During geometry optimization, O atoms of carboxylate groups of the metal binding ligands were frozen to simulate the rigidity of the framework. Minima of all geometry-optimized structures were verified by having no imaginary frequency found from analytical frequency calculation performed at the same level of theory.

RESULTS AND DISCUSSION

Synthesis of the Catalysts. MOF-808 is composed of 12-connected cuboctahedron $Zr_6O_4(OH)_4(-COO)_{12}$ secondary building units (SBUs) linked to the other SBUs by six benzenetricarboxylates (BTC) with three above and three below the ring of formates to form tetrahedral cages (Figure 1a). When linked, these cages form an adamantane-shaped pore with formate, water, and hydroxide molecules completing the coordination spheres of Zr(IV) and pointing into the pseudohexagonal pore openings (Figure 1b). Replacement of these formate, water, or hydroxide molecules with imidazole-based ligands bearing carboxylic acid functionality will result in imidazole units localizing in the center of the pores. These ligands are spatially and precisely positioned for stabilizing copper−oxygen species in the framework (Figure 1c).

Specifically, we synthesized microcrystalline MOF-808 to allow for a facile diffusion of substrates during postsynthetic modifications and catalysis.[39] We selected three different metal binding ligands comprising biologically relevant imidazole units for incorporation into the framework to demonstrate the modularity of our system and to study the effects of ligand on the catalytic properties. Metal binding ligands including L-histidine (His), 4-imidazoleacrylic acid (Iza), and 5-benzimidazolecarboxylic acid (Bzz) were incorporated into the framework by heating MOF-808 in saturated solutions of these metal binding ligands to produce MOF-808-L with -L being -His, -Iza, and -Bzz, respectively. The successful substitution of formate with these ligands in the MOF was confirmed by ^{1}H nuclear magnetic resonance (NMR) of the digested samples (section S2.1). Of the six available sites per

DOI: 10.1021/jacs.8b11525
J. Am. Chem. Soc. 2018, 140, 18208−18216

chemical formula, approximately one-half of these were exchanged with the metal binding ligands to produce MOF-808-His $[Zr_6O_4(OH)_4(BTC)_2(His)_{3.5}(OH)_{2.5}(H_2O)_{2.5}]$, MOF-808-Iza $[Zr_6O_4(OH)_4(BTC)_2(Iza)_{3.7}(HCOO)_{1.6}(OH)_{0.7}(H_2O)_{0.7}]$, and MOF-808-Bzz $[Zr_6O_4(OH)_4(BTC)_2(Bzz)_{3.4}(HCOO)_{1.6}(OH)_1(H_2O)_1]$. Similar procedures were performed on single crystals of MOF-808 for structural elucidation of these functionalized MOFs. Single-crystal X-ray diffraction (SXRD) analysis reveals that these ligands bind to the Zr clusters in a bridging fashion with carboxylate group coordinating to Zr(IV) (section S4) and thus placing imidazole units in the center of the pseudohexagonal window. Metalation of these MOFs with CuI in ACN under air at room temperature provides the catalysts, MOF-808-His-Cu, MOF-808-Iza-Cu, and MOF-808-Bzz-Cu. Inductively coupled plasma atomic emission spectroscopy (ICP-AES) analysis performed on these catalysts indicates the Cu/Zr_6 molar ratios of 4.9, 6.0, and 7.1 for MOF-808-His-Cu, MOF-808-Iza-Cu, and MOF-808-Bzz-Cu, respectively (Table 1). A control experiment was performed by metalation of MOF-808 under similar conditions. Negligible incorporation of copper was observed (Cu/Zr_6 molar ratio = 0.3), suggesting the role of imidazole ligands in ligating to copper atoms. The phase purity and crystallinity of the materials after postsynthetic modifications were preserved as confirmed by powder X-ray diffraction (PXRD) analysis (section S2.2). The porosity of these materials was verified by N_2 adsorption–desorption isotherm measurements at 77 K with BET surface areas of 385, 580, and 580 $m^2\ g^{-1}$ for MOF-808-His-Cu, MOF-808-Iza-Cu, and MOF-808-Bzz-Cu, respectively (section S2.3).

Table 1. Summary of Catalyst Compositions

catalyst	L/Zr_6 molar ratio	Cu/Zr_6 molar ratio	Cu/L molar ratio
MOF-808-His-Cu	3.5	4.9	1.4
MOF-808-Iza-Cu	3.7	6.0	1.6
MOF-808-Bzz-Cu	3.4	7.1	2.1
MOF-808-Cu		0.3	

Methane Oxidation. Methane oxidation was conducted with an isothermal series of treatments at 150 °C. First, 100 mg of MOF-808-L-Cu catalyst was pretreated in He flow to remove residual solvents (i.e., ACN and water) at temperatures starting from room temperature to 150 °C at a ramping rate of 3 °C min^{-1}. After a clean background was achieved by monitoring the signals from a gas chromatograph, the catalyst was treated with 3% N_2O/He for 2 h at 150 °C followed by purging the catalyst with He for 30 min. The catalyst was subsequently exposed to a flow of CH_4 for 1 h at 150 °C for methane activation. After He purge, water was introduced in the form of 3% steam in He at 150 °C to desorb methanol. As shown in Figure 2a, the average methanol productivity corresponds to 31.7 ± 13.0, 61.8 ± 17.5, and 71.8 ± 23.4 μmol $g_{MOF\text{-}808\text{-}L\text{-}Cu}^{-1}$ for MOF-808-His-Cu, MOF-808-Iza-Cu, and MOF-808-Bzz-Cu, respectively, indicating that the MOF-808-Bzz-Cu has the highest methanol productivity among three catalysts. In terms of the turnover numbers (methanol productivity per mole of copper), MOF-808-His-Cu exhibited

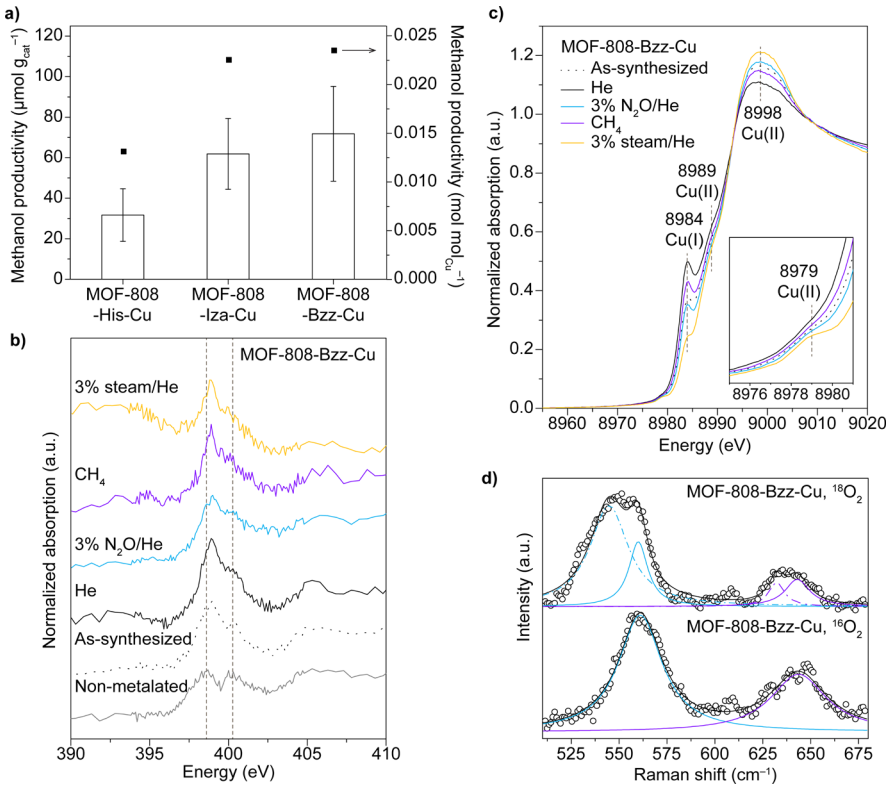

Figure 2. (a) Average with standard error of methanol productivity of MOF-808-His-Cu, MOF-808-Iza-Cu, and MOF-808-Bzz-Cu. (b) Ex situ N K-edge XANES spectra of MOF-808-Bzz, as-synthesized MOF-808-Bzz-Cu, and MOF-808-Bzz-Cu after the reactions with He, 3% N_2O/He, CH_4, and 3% steam/He. (c) Ex situ Cu K-edge XANES spectra of MOF-808-Bzz-Cu after the reactions with He, 3% N_2O/He, CH_4, and 3% steam/He. (d) Resonance Raman spectra of MOF-808-Bzz-Cu synthesized using $^{16}O_2$ and $^{18}O_2$ with 407 nm laser. Note that the $^{18}O_2$ spectrum contains some $^{16}O_2$ contamination.

DOI: 10.1021/jacs.8b11525
J. Am. Chem. Soc. 2018, 140, 18208–18216

lower activity, which is more likely due to lower number of catalytically active copper−oxygen species (~43% lower turnover number as compared to MOF-808-Bzz-Cu), attributed to the flexibility of histidine ligand. Another possible reason is related to the electronic properties of the active site, which will be discussed below.

Notably, only methanol and water were observed as products during methanol desorption at temperatures below or equal to 150 °C. This was confirmed by gas chromatographs equipped with flame ionization and thermal conductivity detectors and a mass analyzer. Above this temperature, we observed increased methanol production with temperature, as we expected due to improved methanol extraction efficiency. However, CO_2 was also observed as a byproduct from the overoxidation of the methanol generated (Figure S27). For the control experiments, we did not observe any products in the experiments performed on MOF-808-L and CuI (Cu(I) precursor in this study).

We examined the structural integrity of the catalysts after the reactions. The crystallinity of the catalysts was maintained as evidenced by PXRD (Figure S14). Interestingly, unlike molecular copper−oxygen complexes,[19] ligand hydroxylation was not observed from digested ^{1}H NMR of the catalysts even at 150 °C, highlighting the significantly enhanced stability imposed by covalent attachment of the complexes that are geometrically constrained in the MOF.

We performed a recyclability test on MOF-808-Bzz-Cu with an isothermal series of treatment at 150 °C (Figure S28). A drastic deactivation was observed in the second and third cycles, giving methanol productivities of 7.5 and 0.1 μmol g^{-1}, respectively. After the third cycle, MOF-808-Bzz-Cu was subjected to a flow of He by increasing the temperature from 150 to 250 °C at a ramping rate of 3 °C min^{-1} and holding for 10 min. Desorbed water was observed during this He treatment until the temperature reached 250 °C. We then proceeded with the isothermal series of treatments at 150 °C; the catalyst showed methanol productivity of 5.4 μmol g^{-1}, which is similar to the productivity obtained from the second cycle. This result indicates that the catalyst deactivation is due to water molecules strongly bound to the active site. We also performed the recyclability test of MOF-808-His-Cu. There is a 77% decrease in methanol productivity from 28 μmol g^{-1} in the first cycle to 6.3 μmol g^{-1} in the second cycle (Figure S29). Unlike MOF-808-Bzz-Cu, the histidine-derived catalyst still exhibits methanol productivity in the third and fourth cycles with 17% and 12% decreases per cycle. Even though there is a recyclability problem in MOF-808-L-Cu catalysts, it is noteworthy that this catalyst shows the highest reported methanol productivity at 71.8 μmol g^{-1} with an isothermal series of treatments at 150 °C with high selectivity to methanol.[48]

Identification of the Active Site in MOF-808-L-Cu. To elucidate the identity of the active site of the catalysts, we synthesized single crystals of MOF-808-L-Cu catalysts following similar procedures employed for microcrystalline samples. However, the active sites of the catalysts are crystallographically disordered, prohibiting an unambiguous structural characterization using SXRD analysis (section S4). We therefore employed element- and structure-specific techniques to determine the structures of the active sites. Energy-dispersive X-ray spectroscopy (EDS) analysis of the catalysts shows a uniform distribution of Zr, N, and Cu atoms throughout the crystals, thus precluding the localization of the active sites on the surface of the MOF crystals (section S2.5).

We carried out N K-edge X-ray absorption near edge structure (XANES), Cu K-edge X-ray absorption spectroscopy (XAS), UV−vis diffuse reflectance spectroscopy (DRS), and resonance Raman spectroscopy measurements on three MOF-808-L-Cu catalysts (detailed spectroscopic data can be found in the Supporting Information). These catalysts show similar trends in the spectroscopic features unless otherwise noted. We therefore use MOF-808-Bzz-Cu as a representative in the following discussion. Comparison of N K-edge XANES spectra of MOF-808-Bzz and MOF-808-Bzz-Cu provides insight into the location of copper in the MOF catalysts (Figure 2b). Two absorption bands at 398.8 and 400.6 eV are observed, assignable to the 1s → π^* transitions of the nitrogen atoms in C−NH−C and C−N=C of imidazole ring, respectively.[49] After the metalation, two absorption peaks are shifted and changed in intensity, indicating that Cu atoms are coordinated to N atoms that are part of the imidazole units. Ex situ N K-edge XANES measurements of the samples after each step of the series of treatments show that two absorption bands remain similar. This indicates that the Cu atoms are coordinated to N atoms throughout the catalytic process.

Ex situ Cu K-edge XANES measurements were performed to probe the oxidation states of copper during catalysis (Figure 2c). Four characteristic peaks located at 8979, 8984, 8989, and 8998 eV are observed. The pre-edge region is shown in the inset of Figure 2c showing a weak absorption peak around 8979 eV corresponding to a dipole-forbidden Cu(II) 1s → 3d electronic transition.[50] The shoulder peak at 8989 eV is attributable to the Cu(II) 1s → 4p + L shakedown transition.[51,52] The Cu(I) 1s → 4p + L shakedown feature is observed at 8984 eV.[53] These data suggest that the catalysts are composed of a mixture of Cu(I) and Cu(II) species. The He pretreatment at 150 °C resulted in a decrease in the white line intensity at 8998 eV along with an increase in the absorption peak intensity at 8984 eV showing that the majority of Cu(II) is reduced to Cu(I) by autoreduction.[54,55] The spectrum recorded after 3% N_2O/He at 150 °C exhibits oxidation of Cu(I) to Cu(II), indicative of the formation of the active copper−oxygen species. After the reaction with methane at 150 °C, the peak intensity of Cu(I) at 8984 eV increased while the white line intensity decreased, suggesting the reduction of Cu(II) to Cu(I).

This reduction could be ascribed to either homolytic cleavage C−H bond followed by direct radical rebound route[56] or Lewis acid/base pair adsorption of methane where oxygen atoms of the active copper−oxygen species reacted with methane.[7,57] After methanol desorption was performed by flowing 3% steam/He at 150 °C into the catalyst, the white line intensity increased accompanied by decreasing intensity of the peak of Cu(I) at 8984 eV. This redox behavior of copper observed from Cu K-edge XANES further proves that the copper active site in our catalysts participates in methane oxidation to methanol. MOF-808-Iza-Cu also shows distinctive changes in the oxidation state of copper following the same trend through the course of the catalytic process as described for MOF-808-Bzz-Cu. MOF-808-His-Cu, however, shows minor intensity changes, consistent with the lower methanol productivity as previously described (Figure 2a).

To gain more information about the active copper−oxygen species, UV−vis DRS was performed. Background subtracted UV−vis DRS spectra of the as-synthesized samples show the

DOI: 10.1021/jacs.8b11525
J. Am. Chem. Soc. 2018, 140, 18208−18216

absorption band centered at ~400 nm. After 3% N_2O/He treatment at 150 °C, we observed the increase of this absorption band (section S5.1) corresponding to oxygen-to-metal charge-transfer transition.[58−61] To definitively characterize this copper−oxygen species, we turned to resonance Raman spectroscopy measurement because each copper−oxygen species have characteristic Raman shifts (section S8).[16,17] We prepared the samples by synthesizing MOF-808-L-Cu in an argon-filled glovebox and oxygenating the samples with either $^{16}O_2$ or $^{18}O_2$ gas at room temperature. Figure 2d shows the isotope-dependent Raman peaks at ~560 and ~640 cm^{-1} by using an excitation wavelength of 407 nm, which is resonant at the charge-transfer band. These peaks are assigned to Cu−O bonds vibration in the core breathing mode of bis(μ-oxo) dicopper species (section S6). In the $^{18}O_2$-labeled samples, these Raman peaks are shifted to ~545 and ~630 cm^{-1}. This isotope-dependent trend is verified for all three MOF-808-L-Cu (Figure 2d and Figures S37 and S39). Ex situ resonance Raman spectroscopy of the samples after the treatments in He and 3% N_2O/He display similar Raman peaks, indicating that bis(μ-oxo) dicopper species are preserved prior to the methane activation. The deviation (~20 cm^{-1}) in the vibrational energy from the reported values[17] can be ascribed to the variation in the geometric parameters of the dicopper species due to the framework constraints.

With the information on the location of the ligands (section S4) and the identity of active copper−oxygen sites, we modeled the active sites using the framework as a constraint and geometrically optimized the models using density functional theory (DFT) calculations. Following the digested ^{1}H NMR data where ~3 ligand molecules were incorporated per chemical formula, these ligands were placed on the Zr cluster on the pseudohexagonal window in a way such that these ligands pose a minimal steric hindrance to each other. Cu atoms were then allowed to coordinate to N atoms of imidazole units, and the Cu atoms were further coordinated to O_2 to form N−Cu_2O_2−N species (section S6). Geometrical optimization indicates that bis(μ-oxo) dicopper species can reside in the framework in all MOF-808-L-Cu structures (Figure 3). Of particular note, the Raman shifts relevant to O_2 are in close agreement with the experimental data, confirming the presence of bis(μ-oxo) dicopper species in the catalysts (section S6).

Figure 4 depicts the k^2-weighted and Fourier transforms without phase correction of the extended X-ray absorption fine structure (EXAFS) data measured at the Cu K-edge of the MOF-808-Bzz-Cu. The spectra were recorded after the successive treatment with (a) He, (b) 3% N_2O/He, (c) CH_4, and (d) 3% steam/He at 150 °C. We used the DFT-optimized cluster as a model to fit the experimental Cu EXAFS spectra. The full EXAFS data were analyzed in k- and R-space using a combined k^1-k^2-k^3 fitting procedure for reliable analysis.[62] The best fits are presented in Figure 4, and the respective fitted parameters are reported in Table 2. In the He treated sample, the first shell is assigned to Cu−N/(O) coordination with the coordination number of 2.9 at distance of 1.94 Å. It should be noted that N and O atoms are indistinguishable from EXAFS analysis as they have similar atomic scattering factors. For the second shell, we identified the scatterer by fitting the EXAFS data with Cu, C, N, and O, and only Cu could be fitted with reasonable fitting statistics. Copper was found at a distance of 2.51 Å with the coordination number of 0.6. This result suggests that the copper site is present as dinuclear, and a short distance of Cu···Cu supports the presence of bis(μ-oxo) dicopper species. Contrary to a formal Cu(III) oxidation state typically assigned for bis(μ-oxo) dicopper species,[63,64] the oxidation state of

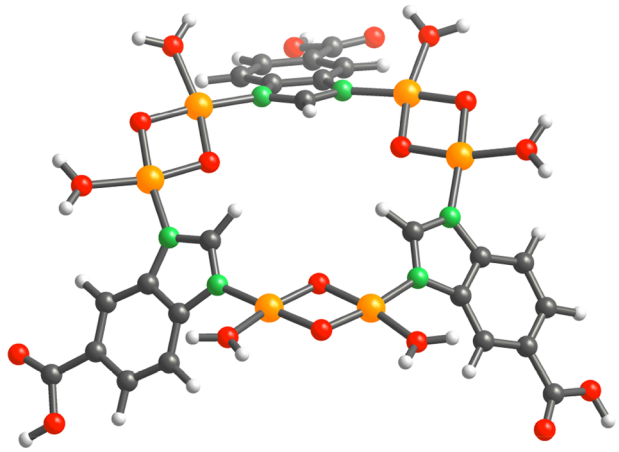

Figure 3. DFT optimized structure of the proposed active site in MOF-808-Bzz-Cu. From ICP, ^{1}H NMR, and N K-edge XANES, each N atom of the ligands is coordinated to one copper atom. However, copper in bis(μ-oxo) dicopper is known to be four-coordinated.[17] We propose that the fourth ligand coordinating to copper is a neutral ligand such as water or *N*,*N*-dimethylformamide molecules as we observed the latter molecule in the ^{1}H NMR spectra of the digested samples after activation (only the optimized structure of the active site is shown, while the remaining atoms of the MOF-808 are omitted for clarity). Atom labeling scheme: C, black; O, red; N, green; H, white; Cu, orange.

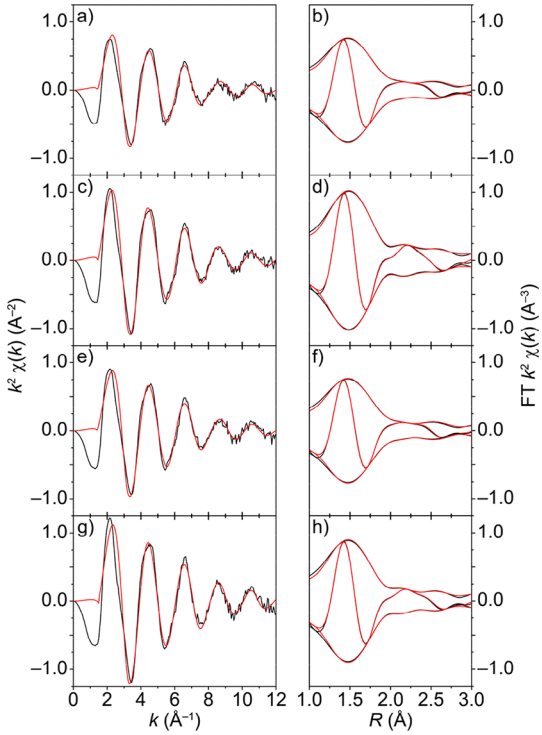

Figure 4. Series of k^2-weighted Cu-EXAFS spectra of MOF-808-Bzz-Cu (black line) and best fit (red line) in k-space (left) and R-space (right) without phase correction after the reactions with (a,b) He, (c,d) 3% N_2O/He, (e,f) CH_4, and (g,h) 3% steam/He at 150 °C. Fitting was conducted using N scatter. Fit range, $3 < k < 10$ Å^{-1}; $1 < R < 4$ Å; fit window, Hanning.

DOI: 10.1021/jacs.8b11525
J. Am. Chem. Soc. 2018, 140, 18208−18216

Table 2. Cu EXAFS Fitting Result of MOF-808-Bzz-Cu with a Series of Treatments

Ab−Sc pair[a]	N[b]	R[c]	DWF[d]	R-factor[e]
MOF-808-Bzz-Cu, He Treated at 150 °C				
Cu−N/(O) SS[f]	2.9	1.94 ± 0.02	0.0080 ± 0.0025	0.019
Cu···Cu SS	0.6	2.51 ± 0.04	0.0146 ± 0.0065	
MOF-808-Bzz-Cu, N_2O Treated at 150 °C				
Cu−N/(O) SS	3.7	1.94 ± 0.02	0.0070 ± 0.0025	0.021
Cu···Cu SS	0.4	2.49 ± 0.10	0.0156 ± 0.0149	
MOF-808-Bzz-Cu, CH_4 Treated at 150 °C				
Cu−N/(O) SS	3.3	1.94 ± 0.02	0.0072 ± 0.0025	0.020
Cu···Cu SS	0.5	2.51 ± 0.07	0.0151 ± 0.0102	
MOF-808-Bzz-Cu, Steam Treated at 150 °C				
Cu−N/(O) SS	3.9	1.95 ± 0.01	0.0058 ± 0.0022	0.018
Cu···Cu SS	0.5	2.53 ± 0.10	0.0169 ± 0.0151	

[a]Ab = absorber; Sc = scatterer. [b]Coordination number. [c]Distance (Å). [d]Debye−Waller factor (Å^2). [e]A measure of mean square sum of the misfit at each data point. [f]SS = single scattering. Fitting was conducted using N scatter. Fit range: $3 < k < 10$ Å^{-1}; $1 < R < 4$ Å. Fit window: Hanning.

active copper in our catalysts appears to be close to Cu(II). This discrepancy can be ascribed to the high electron density provided by the imidazole ligand to the Cu centers. The bond valence sum analysis (BVS) (Tables S5−S7) further indicates the actual charge being close to 2-fold.[53,65,66] Oxidation of the catalyst in 3% N_2O/He at 150 °C leads to 0.8 increase of the Cu−N/(O) coordination while its distance remains at 1.94 Å, indicating the additional formation of bis(μ-oxo) dicopper species. BVS analysis further sheds light on the difference in electronic properties leading to varying catalytic properties among three catalysts. From this analysis, the oxidation state of copper in MOF-808-His-Cu is slightly lower than those in MOF-808-Iza-Cu and MOF-808-Bzz-Cu, which agrees with the trend of Mulliken charges of these catalysts determined from DFT calculations (Figures S49−S51). These results suggest that Cu active sites in MOF-808-His-Cu have lower oxidizing power as compared to the other two. After methane treatment, there is a slight decrease in Cu−N/(O) coordination, and, after methanol extraction, Cu−N/(O) coordination increases by 0.6. However, Cu−N/(O) coordination in MOF-808-His-Cu and MOF-808-Iza-Cu remains similar after treatment with methane and steam.

CONCLUSION

We show that, by selection of MOF with appropriate structure and topology, MOF-808 can be utilized as a scaffold to host and stabilize highly active copper−oxygen complexes, bis(μ-oxo) dicopper species, ligated to biologically relevant imidazole moieties including L-histidine (His), 4-imidazoleacrylic acid (Iza), and 5-benzimidazolecarboxylic acid (Bzz) inspired by pMMO. The catalysts show high selectivity for methane oxidation to methanol under isothermal condition at 150 °C. We anticipate that the strategy reported here will serve as a blueprint for other bioinspired catalysts in MOFs for a broad array of catalytic transformations.

ASSOCIATED CONTENT

Supporting Information

The Supporting Information is available free of charge on the ACS Publications website at DOI: 10.1021/jacs.8b11525.

Detailed description of synthesis, materials characterization, catalysis, single-crystal X-ray diffraction analyses, UV−vis diffuse reflectance and resonance Raman spectroscopy, density functional theory calculations, X-ray absorption spectroscopy, charge distribution, and identification of the active site (PDF)

X-ray crystallographic data for MOF-808-His (CIF)

X-ray crystallographic data for MOF-808-Iza (CIF)

X-ray crystallographic data for MOF-808-Bzz (CIF)

AUTHOR INFORMATION

Corresponding Authors

*somorjai@berkeley.edu

*yaghi@berkeley.edu

ORCID

Jayeon Baek: 0000-0002-4183-6299

Myeongkee Park: 0000-0002-5307-2564

Roc Matheu: 0000-0001-8601-5219

Gabor A. Somorjai: 0000-0002-8478-2761

Omar M. Yaghi: 0000-0002-5611-3325

Author Contributions

○J.B. and B.R. contributed equally to this work.

Notes

The authors declare no competing financial interest.

ACKNOWLEDGMENTS

The research performed in the O.M.Y. laboratory was supported by BASF SE (Ludwigshafen, Germany) and King Abdulaziz City for Science and Technology. G.A.S. acknowledges support from the Director, Office of Basic Energy Sciences, Division of Chemical Sciences, Geological and Biosciences of the U.S. Department of Energy under contract no. DE-AC02-05CH11231. Research work at the Molecular Foundry was supported by the Office of Science, Office of Basic Energy Sciences, of the DOE under contract no. DE-AC02-05CH11231. The Advanced Light Source (ALS) is supported by the Director, Office of Science, Office of Basic Energy Sciences, of the U.S. Department of Energy under contract DE-AC02-05CH11231. The Molecular Graphics and Computation Facility is funded by the NIH (S10OD023532). The AVB-400 NMR spectrometer is partially supported by NSF Grant CHE-0130862. We thank Drs. Philipp Urban, Dave Small, Kathleen A. Durkin, Georgios Katsoukis, and Tae Yong Kim for discussions and Drs. Simon J. Teat and Laura J. McCormick for synchrotron X-ray diffraction data acquisition support. B.R. is supported by the Royal Thai Government Scholarship.

REFERENCES

(1) Periana, R. A.; Taube, D. J.; Evitt, E. R.; Löffler, D. G.; Wentrcek, P. R.; Voss, G.; Masuda, T. A mercury-catalyzed, high-yield system for the oxidation of methane to methanol. *Science* **1993**, *259* (5093), 340−343.

(2) Groothaert, M. H.; Smeets, P. J.; Sels, B. F.; Jacobs, P. A.; Schoonheydt, R. A. Selective oxidation of methane by the bis(μ-oxo) dicopper core stabilized on ZSM-5 and mordenite zeolites. *J. Am. Chem. Soc.* **2005**, *127* (5), 1394−1395.

(3) Woertink, J. S.; Smeets, P. J.; Groothaert, M. H.; Vance, M. A.; Sels, B. F.; Schoonheydt, R. A.; Solomon, E. I. A $[Cu2O]^{2+}$ core in Cu-ZSM-5, the active site in the oxidation of methane to methanol. *Proc. Natl. Acad. Sci. U. S. A.* **2009**, *106* (45), 18908−18913.

(4) Hammond, C.; Forde, M. M.; Rahim, A.; Hasbi, M.; Thetford, A.; He, Q.; Jenkins, R. L.; Dimitratos, N.; Lopez-Sanchez, J. A.; Dummer, N. F. Direct Catalytic Conversion of Methane to Methanol in an Aqueous Medium by using Copper-Promoted Fe-ZSM-5. *Angew. Chem., Int. Ed.* **2012**, *51* (21), 5129−5133.
(5) Grundner, S.; Markovits, M. A.; Li, G.; Tromp, M.; Pidko, E. A.; Hensen, E. J.; Jentys, A.; Sanchez-Sanchez, M.; Lercher, J. A. Single-site trinuclear copper oxygen clusters in mordenite for selective conversion of methane to methanol. *Nat. Commun.* **2015**, *6*, 7546.
(6) Narsimhan, K.; Iyoki, K.; Dinh, K.; Román-Leshkov, Y. Catalytic oxidation of methane into methanol over copper-exchanged zeolites with oxygen at low temperature. *ACS Cent. Sci.* **2016**, *2* (6), 424−429.
(7) Sushkevich, V. L.; Palagin, D.; Ranocchiari, M.; van Bokhoven, J. A. Selective anaerobic oxidation of methane enables direct synthesis of methanol. *Science* **2017**, *356* (6337), 523−527.
(8) Tomkins, P.; Mansouri, A.; Bozbag, S. E.; Krumeich, F.; Park, M. B.; Alayon, E. M. C.; Ranocchiari, M.; van Bokhoven, J. A. Isothermal Cyclic Conversion of Methane into Methanol over Copper-Exchanged Zeolite at Low Temperature. *Angew. Chem.* **2016**, *128* (18), 5557−5561.
(9) Lawton, T. J.; Rosenzweig, A. C. Methane-oxidizing enzymes: an upstream problem in biological gas-to-liquids conversion. *J. Am. Chem. Soc.* **2016**, *138* (30), 9327−9340.
(10) Ravi, M.; Ranocchiari, M.; van Bokhoven, J. A. A Critical Assessment of the Direct Catalytic Oxidation of Methane to Methanol. *Angew. Chem., Int. Ed.* **2017**, *56* (52), 16464−16483.
(11) Schoedel, A.; Ji, Z.; Yaghi, O. M. The role of metal−organic frameworks in a carbon-neutral energy cycle. *Nature Energy* **2016**, *1*, 16034.
(12) Balasubramanian, R.; Smith, S. M.; Rawat, S.; Yatsunyk, L. A.; Stemmler, T. L.; Rosenzweig, A. C. Oxidation of methane by a biological dicopper centre. *Nature* **2010**, *465* (7294), 115.
(13) Culpepper, M. A.; Cutsail, G. E., III; Hoffman, B. M.; Rosenzweig, A. C. Evidence for oxygen binding at the active site of particulate methane monooxygenase. *J. Am. Chem. Soc.* **2012**, *134* (18), 7640−7643.
(14) Culpepper, M. A.; Cutsail, G. E., III; Gunderson, W. A.; Hoffman, B. M.; Rosenzweig, A. C. Identification of the valence and coordination environment of the particulate methane monooxygenase copper centers by advanced EPR characterization. *J. Am. Chem. Soc.* **2014**, *136* (33), 11767−11775.
(15) Cao, L.; Caldararu, O.; Rosenzweig, A. C.; Ryde, U. Quantum Refinement Does Not Support Dinuclear Copper Sites in Crystal Structures of Particulate Methane Monooxygenase. *Angew. Chem., Int. Ed.* **2018**, *57* (1), 162−166.
(16) Elwell, C. E.; Gagnon, N. L.; Neisen, B. D.; Dhar, D.; Spaeth, A. D.; Yee, G. M.; Tolman, W. B. Copper−oxygen complexes revisited: structures, spectroscopy, and reactivity. *Chem. Rev.* **2017**, *117* (3), 2059−2107.
(17) Mirica, L. M.; Ottenwaelder, X.; Stack, T. D. P. Structure and spectroscopy of copper−dioxygen complexes. *Chem. Rev.* **2004**, *104* (2), 1013−1046.
(18) Solomon, E. I.; Ginsbach, J. W.; Heppner, D. E.; Kieber-Emmons, M. T.; Kjaergaard, C. H.; Smeets, P. J.; Tian, L.; Woertink, J. S. Copper dioxygen (bio) inorganic chemistry. *Faraday Discuss.* **2011**, *148*, 11−39.
(19) Citek, C.; Herres-Pawlis, S.; Stack, T. D. P. Low temperature syntheses and reactivity of Cu_2O_2 active-site models. *Acc. Chem. Res.* **2015**, *48* (8), 2424−2433.
(20) Que, L., Jr; Tolman, W. B. Bis(μ-oxo) dimetal "Diamond" Cores in Copper and Iron Complexes Relevant to Biocatalysis. *Angew. Chem., Int. Ed.* **2002**, *41* (7), 1114−1137.
(21) Pappas, D. K.; Borfecchia, E.; Dyballa, M.; Pankin, I. A.; Lomachenko, K. A.; Martini, A.; Signorile, M.; Teketel, S.; Arstad, B.; Berlier, G. Methane to Methanol: Structure−Activity Relationships for Cu-CHA. *J. Am. Chem. Soc.* **2017**, *139* (42), 14961−14975.
(22) Osadchii, D.; Olivos Suarez, A. I.; Szécsényi, Á.; Li, G.; Nasalevich, M. A.; Dugulan, A. I.; Serra-Crespo, P.; Hensen, E. J.; Veber, S. L.; Fedin, M. V. Isolated Fe sites in Metal Organic Framework catalyze the direct conversion of methane to methanol. *ACS Catal.* **2018**, *8* (6), 5542−5548.
(23) Wang, V. C.-C.; Maji, S.; Chen, P. P.-Y.; Lee, H. K.; Yu, S. S.-F.; Chan, S. I. Alkane oxidation: Methane monooxygenases, related enzymes, and their biomimetics. *Chem. Rev.* **2017**, *117* (13), 8574−8621.
(24) Lu, Y.; Yeung, N.; Sieracki, N.; Marshall, N. M. Design of functional metalloproteins. *Nature* **2009**, *460* (7257), 855.
(25) Lillerud, K. P.; Olsbye, U.; Tilset, M. Designing heterogeneous catalysts by incorporating enzyme-like functionalities into MOFs. *Top. Catal.* **2010**, *53* (13−14), 859−868.
(26) Xiao, D. J.; Bloch, E. D.; Mason, J. A.; Queen, W. L.; Hudson, M. R.; Planas, N.; Borycz, J.; Dzubak, A. L.; Verma, P.; Lee, K. Oxidation of ethane to ethanol by N_2O in a metal−organic framework with coordinatively unsaturated iron (II) sites. *Nat. Chem.* **2014**, *6* (7), 590.
(27) Gu, Z. Y.; Park, J.; Raiff, A.; Wei, Z.; Zhou, H. C. Metal−organic frameworks as biomimetic catalysts. *ChemCatChem* **2014**, *6* (1), 67−75.
(28) Furukawa, H.; Cordova, K. E.; O'Keeffe, M.; Yaghi, O. M. The chemistry and applications of metal-organic frameworks. *Science* **2013**, *341* (6149), 1230444.
(29) Rungtaweevoranit, B.; Diercks, C. S.; Kalmutzki, M. J.; Yaghi, O. M. Spiers Memorial Lecture: Progress and prospects of reticular chemistry. *Faraday Discuss.* **2017**, *201*, 9−45.
(30) Osborn Popp, T. M.; Yaghi, O. M. Sequence-Dependent Materials. *Acc. Chem. Res.* **2017**, *50* (3), 532−534.
(31) Fracaroli, A. M.; Siman, P.; Nagib, D. A.; Suzuki, M.; Furukawa, H.; Toste, F. D.; Yaghi, O. M. Seven post-synthetic covalent reactions in tandem leading to enzyme-like complexity within metal−organic framework crystals. *J. Am. Chem. Soc.* **2016**, *138* (27), 8352−8355.
(32) O'Keeffe, M.; Yaghi, O. M. Deconstructing the crystal structures of metal−organic frameworks and related materials into their underlying nets. *Chem. Rev.* **2012**, *112* (2), 675−702.
(33) Lee, S.; Kapustin, E. A.; Yaghi, O. M. Coordinative alignment of molecules in chiral metal-organic frameworks. *Science* **2016**, *353* (6301), 808−811.
(34) Deria, P.; Mondloch, J. E.; Tylianakis, E.; Ghosh, P.; Bury, W.; Snurr, R. Q.; Hupp, J. T.; Farha, O. K. Perfluoroalkane functionalization of NU-1000 via solvent-assisted ligand incorporation: synthesis and CO_2 adsorption studies. *J. Am. Chem. Soc.* **2013**, *135* (45), 16801−16804.
(35) Yuan, S.; Lu, W.; Chen, Y.-P.; Zhang, Q.; Liu, T.-F.; Feng, D.; Wang, X.; Qin, J.; Zhou, H.-C. Sequential linker installation: precise placement of functional groups in multivariate metal−organic frameworks. *J. Am. Chem. Soc.* **2015**, *137* (9), 3177−3180.
(36) Manna, K.; Zhang, T.; Lin, W. Postsynthetic metalation of bipyridyl-containing metal−organic frameworks for highly efficient catalytic organic transformations. *J. Am. Chem. Soc.* **2014**, *136* (18), 6566−6569.
(37) Doonan, C. J.; Morris, W.; Furukawa, H.; Yaghi, O. M. Isoreticular Metalation of Metal− Organic Frameworks. *J. Am. Chem. Soc.* **2009**, *131* (27), 9492−9493.
(38) Furukawa, H.; Gándara, F.; Zhang, Y.-B.; Jiang, J.; Queen, W. L.; Hudson, M. R.; Yaghi, O. M. Water adsorption in porous metal−organic frameworks and related materials. *J. Am. Chem. Soc.* **2014**, *136* (11), 4369−4381.
(39) Choi, K. M.; Jeong, H. M.; Park, J. H.; Zhang, Y.-B.; Kang, J. K.; Yaghi, O. M. Supercapacitors of nanocrystalline metal−organic frameworks. *ACS Nano* **2014**, *8* (7), 7451−7457.
(40) Marcus, M. A.; MacDowell, A. A.; Celestre, R.; Manceau, A.; Miller, T.; Padmore, H. A.; Sublett, R. E. Beamline 10.3. 2 at ALS: a hard X-ray microprobe for environmental and materials sciences. *J. Synchrotron Radiat.* **2004**, *11* (3), 239−247.
(41) Kraft, S.; Stümpel, J.; Becker, P.; Kuetgens, U. High resolution x-ray absorption spectroscopy with absolute energy calibration for the determination of absorption edge energies. *Rev. Sci. Instrum.* **1996**, *67* (3), 681−687.

DOI: 10.1021/jacs.8b11525
J. Am. Chem. Soc. 2018, 140, 18208−18216

(42) Kelly, S.; Hesterberg, D.; Ravel, B. Analysis of soils and minerals using X-ray absorption spectroscopy. *Methods of soil analysis. Part 5. Mineralogical methods* **2008**, *5*, 387−464.
(43) Ravel, B.; Newville, M. ATHENA, ARTEMIS, HEPHAESTUS: data analysis for X-ray absorption spectroscopy using IFEFFIT. *J. Synchrotron Radiat.* **2005**, *12* (4), 537−541.
(44) Newville, M. IFEFFIT: interactive XAFS analysis and FEFF fitting. *J. Synchrotron Radiat.* **2001**, *8* (2), 322−324.
(45) Becke, A. D. Density-functional thermochemistry. III. The role of exact exchange. *J. Chem. Phys.* **1993**, *98* (7), 5648−5652.
(46) Lee, C.; Yang, W.; Parr, R. G. Development of the Colle-Salvetti correlation-energy formula into a functional of the electron density. *Phys. Rev. B: Condens. Matter Mater. Phys.* **1988**, *37* (2), 785.
(47) Frisch, M. J.; Trucks, G. W.; Schlegel, H. B.; Scuseria, G. E.; Robb, M. A.; Cheeseman, J. R.; Scalmani, G.; Barone, V.; Petersson, G. A.; Nakatsuji, H.; Li, X.; Caricato, M.; Marenich, A. V.; Bloino, J.; Janesko, B. G.; Gomperts, R.; Mennucci, B.; Hratchian, H. P.; Ortiz, J. V.; Izmaylov, A. F.; Sonnenberg, J. L.; Williams; Ding, F.; Lipparini, F.; Egidi, F.; Goings, J.; Peng, B.; Petrone, A.; Henderson, T.; Ranasinghe, D.; Zakrzewski, V. G.; Gao, J.; Rega, N.; Zheng, G.; Liang, W.; Hada, M.; Ehara, M.; Toyota, K.; Fukuda, R.; Hasegawa, J.; Ishida, M.; Nakajima, T.; Honda, Y.; Kitao, O.; Nakai, H.; Vreven, T.; Throssell, K.; Montgomery, J. A., Jr.; Peralta, J. E.; Ogliaro, F.; Bearpark, M. J.; Heyd, J. J.; Brothers, E. N.; Kudin, K. N.; Staroverov, V. N.; Keith, T. A.; Kobayashi, R.; Normand, J.; Raghavachari, K.; Rendell, A. P.; Burant, J. C.; Iyengar, S. S.; Tomasi, J.; Cossi, M.; Millam, J. M.; Klene, M.; Adamo, C.; Cammi, R.; Ochterski, J. W.; Martin, R. L.; Morokuma, K.; Farkas, O.; Foresman, J. B.; Fox, D. J. *Gaussian 16*, revision A.03; Gaussian, Inc.: Wallingford, CT, 2016.
(48) Ikuno, T.; Zheng, J.; Vjunov, A.; Sanchez-Sanchez, M.; Ortuño, M. A.; Pahls, D. R.; Fulton, J. L.; Camaioni, D. M.; Li, Z.; Ray, D. Methane Oxidation to Methanol Catalyzed by Cu-oxo Clusters Stabilized in NU-1000 Metal−Organic Framework. *J. Am. Chem. Soc.* **2017**, *139* (30), 10294−10301.
(49) Zubavichus, Y.; Shaporenko, A.; Grunze, M.; Zharnikov, M. Innershell absorption spectroscopy of amino acids at all relevant absorption edges. *J. Phys. Chem. A* **2005**, *109* (32), 6998−7000.
(50) Kau, L. S.; Spira-Solomon, D. J.; Penner-Hahn, J. E.; Hodgson, K. O.; Solomon, E. I. X-ray absorption edge determination of the oxidation state and coordination number of copper. Application to the type 3 site in Rhus vernicifera laccase and its reaction with oxygen. *J. Am. Chem. Soc.* **1987**, *109* (21), 6433−6442.
(51) Shadle, S. E.; Penner-Hahn, J. E.; Schugar, H. J.; Hedman, B.; Hodgson, K. O.; Solomon, E. I. X-ray absorption spectroscopic studies of the blue copper site: metal and ligand K-edge studies to probe the origin of the EPR hyperfine splitting in plastocyanin. *J. Am. Chem. Soc.* **1993**, *115* (2), 767−776.
(52) Kau, L. S.; Hodgson, K. O.; Solomon, E. I. X-ray absorption edge and EXAFS study of the copper sites in zinc oxide methanol synthesis catalysts. *J. Am. Chem. Soc.* **1989**, *111* (18), 7103−7109.
(53) Groothaert, M. H.; van Bokhoven, J. A.; Battiston, A. A.; Weckhuysen, B. M.; Schoonheydt, R. A. Bis(μ-oxo) dicopper in Cu-ZSM-5 and its role in the decomposition of NO: a combined in situ XAFS, UV− Vis− Near-IR, and kinetic study. *J. Am. Chem. Soc.* **2003**, *125* (25), 7629−7640.
(54) Trout, B. L.; Chakraborty, A. K.; Bell, A. T. Local spin density functional theory study of copper ion-exchanged ZSM-5. *J. Phys. Chem.* **1996**, *100* (10), 4173−4179.
(55) Alayon, E. M. C.; Nachtegaal, M.; Bodi, A.; Ranocchiari, M.; van Bokhoven, J. A. Bis(μ-oxo) versus mono (μ-oxo) dicopper cores in a zeolite for converting methane to methanol: an in situ XAS and DFT investigation. *Phys. Chem. Chem. Phys.* **2015**, *17* (12), 7681−7693.
(56) Li, G.; Vassilev, P.; Sanchez-Sanchez, M.; Lercher, J. A.; Hensen, E. J.; Pidko, E. A. Stability and reactivity of copper oxo-clusters in ZSM-5 zeolite for selective methane oxidation to methanol. *J. Catal.* **2016**, *338*, 305−312.
(57) Olivos-Suarez, A. I.; Szécsényi, A. g.; Hensen, E. J.; Ruiz-Martinez, J.; Pidko, E. A.; Gascon, J. Strategies for the direct catalytic valorization of methane using heterogeneous catalysis: challenges and opportunities. *ACS Catal.* **2016**, *6* (5), 2965−2981.
(58) Mahadevan, V.; Hou, Z.; Cole, A. P.; Root, D. E.; Lal, T. K.; Solomon, E. I.; Stack, T. Irreversible Reduction of Dioxygen by Simple Peralkylated Diamine−Copper (I) Complexes: Characterization and Thermal Stability of a $[Cu_2(\mu\text{-}O)^{2]2+}$ Core. *J. Am. Chem. Soc.* **1997**, *119* (49), 11996−11997.
(59) Kang, P.; Bobyr, E.; Dustman, J.; Hodgson, K. O.; Hedman, B.; Solomon, E. I.; Stack, T. D. P. Bis(μ-oxo) dicopper (III) species of the simplest peralkylated diamine: enhanced reactivity toward exogenous substrates. *Inorg. Chem.* **2010**, *49* (23), 11030−11038.
(60) Smeets, P. J.; Hadt, R. G.; Woertink, J. S.; Vanelderen, P.; Schoonheydt, R. A.; Sels, B. F.; Solomon, E. I. Oxygen precursor to the reactive intermediate in methanol synthesis by Cu-ZSM-5. *J. Am. Chem. Soc.* **2010**, *132* (42), 14736−14738.
(61) Kim, Y.; Kim, T. Y.; Lee, H.; Yi, J. Distinct activation of Cu-MOR for direct oxidation of methane to methanol. *Chem. Commun.* **2017**, *53* (29), 4116−4119.
(62) Tromp, M.; van Bokhoven, J. A.; Arink, A. M.; Bitter, J. H.; van Koten, G.; Koningsberger, D. C. Cu K-Edge EXAFS Characterisation of Copper (I) Arenethiolate Complexes in both the Solid and Liquid State: Detection of Cu−Cu Coordination. *Chem. - Eur. J.* **2002**, *8* (24), 5667−5678.
(63) Herres-Pawlis, S.; Verma, P.; Haase, R.; Kang, P.; Lyons, C. T.; Wasinger, E. C.; Flörke, U.; Henkel, G.; Stack, T. D. P. Phenolate hydroxylation in a bis(μ-oxo) dicopper (III) complex: lessons from the guanidine/amine series. *J. Am. Chem. Soc.* **2009**, *131* (3), 1154−1169.
(64) DuBois, J. L.; Mukherjee, P.; Stack, T.; Hedman, B.; Solomon, E. I.; Hodgson, K. O. A systematic K-edge X-ray absorption spectroscopic study of Cu (III) sites. *J. Am. Chem. Soc.* **2000**, *122* (24), 5775−5787.
(65) Hati, S.; Datta, D. Nature of the active sites in haemocyanin and iron nickel hydrogenases: the bond valence sum approach. *J. Chem. Soc., Dalton Trans.* **1995**, No. 7, 1177−1182.
(66) Mahapatra, S.; Halfen, J. A.; Wilkinson, E. C.; Pan, G.; Wang, X.; Young, V. G.; Cramer, C. J.; Que, L.; Tolman, W. B. Structural, spectroscopic, and theoretical characterization of bis(μ-oxo) dicopper complexes, novel intermediates in copper-mediated dioxygen activation. *J. Am. Chem. Soc.* **1996**, *118* (46), 11555−11574.

DOI: 10.1021/jacs.8b11525
J. Am. Chem. Soc. 2018, 140, 18208−18216